The Active Degrader

Ilektra A. Christidi, Stony Brook

June 22, 2006

Abstract

The Active Degrader (AD) has not been used in the PNN1 analysis, but is essential for PNN2, given the expected photon distribution from target-scattered Kp2 events, which is uniform in dip angle ([1], fig. 2 and 3). Sure enough, photon activity is evident for Kp2 and kink events.

1 Formalities

In the following, "energies" are in arbitrary units. For the CCDs they are the pulse height (average of the 2 highest bins of the pulse found by the pulse.f routine) and they have been calibrated with respect to each other and pedestal-corrected for multiple hits in one CCD. For the ADCs they are the ADC hit values, also calibrated with respect to each other and then de-multiplexed based on the CCD information: the CCD energy of all hits in every sector, as well as in every ADC multiplexed unit, is summed, and their ratio gives the contribution of every sector to the ADC energy. This way an ADC value is assigned in every sector (not every hit, unlike the CCD), and then it is corrected also for the energy lost in dead material when multiple sectors are crossed. This effect was observed as a down-shift of about 13 (in ADC units) in the Kaon energy peak for every extra sector crossed. For the CCDs, the energy loss correction is absorbed in the pedestal subtraction.
Beam particle track extrapolation is done to find which AD sectors are expected to be transversed by the incoming K, and thus have some energy deposit associated with the beam. In principle, these sectors should be excluded for PV purposes (more on that later). The incoming xy point is found by extrapolating the line defined by the hit points in BWC1 and BWC2 to the US face of the AD. The outgoing point is the one given by the B4 hit coordinates. Every sector between these 2 points is assigned to the K path. This algorithm has the flaw that it does not take into account the transverse uncertainty to the entering K point caused by multiple scattering in the Inactive Degrader (which is right US of the AD), which is exacerbated by the geometry of the AD: since the beam is centered where all the sectors meet, a small perturbation in the path causes more/other sectors than expected to be hit. A quantitative assessment of the efficiency of the method is given later.
When slewing corrections based on the incoming beam Kaon were applied to the TDCs and CCDs, the time resolution for the K was not improved significantly but the distributions for the photons were distorted. This might be due to several reasons: (a) the K deposits most of its energy towards the DS of the AD, when it slows down, whereas the photons deposit it more towards the US, when they shower (or at least more uniformly in z than the K). Since we do not know the z-dependence of

the gain, this can cause a slewing correction derived from K's (i.e. mostly from the DS) not to work for photons. To check this hypothesis, slewing corrections based on beam pions (that deposit energy more uniformly in z) are being investigated. (b) the K beam is more or less centered at the AD, whereas the photons can be anywhere in xy. Since the gain changes by up to a factor of 3 from the center to the edge, this can be another source of discrepancy, which could not be disentangled (we have no position information for the outgoing photons). The time slewing studies will be repeated for a fixed radius of the incoming K, to check this scenario. (c) the slewing corrections were derived from events in which the K transverses only one sector. This is not a representative sample, and an unknown amount of the energy could be lost in dead material (among other unpredictable features). The study will be repeated with events with 2 and 3 sectors hit by the K.

The relative timing between different sectors fluctuated by about 200ps at most, so this was not deemed to be a neccessary correction.
The acceptance sample used in these studies is Km21 monitors, with KINCUTS, PSCUT02 and KMU2BOX cut applied, where no photon or beam activity is expected. Two rejection samples were used: Kp2 peak events from SKIM5 (without TDCUT), with KINCUTS, PSCUT02, KPI2BOX, loose PVCUT and TGCUTS, and "good" (kink point in the target) kinks from SKIM8 with SKIM5 cuts (without TDCUT), KINCUTS, PSCUT02_KINK, $ptot < 225MeV/c$, loose PVCUT, loose TGCUTS and DELCO3. The kinematic quantities (rtot, ptot, etot and DELCO) of these samples are shown in fig. 1, before the PV and, for the first 3 quantities, before the BOX cut.

2 Timing peaks in the AD

In fig.2-5, the time distributions of hits in the AD are shown in black for the acceptance sample and red for the rejection samples (Kp2 peak on the left and kinks on the right). All the histograms are normalized to the number of events/incoming Kaons. As can be seen in fig. 2, which is for sectors on the K path, the behaviour of the 3 samples is effectively the same in terms of K activity. The upper plots are the times with respect to tk, where an on-time peak at -0.06ns with 0.8ns sigma (from a Gaussian fit) is obvious, and the lower ones with respect to tpi, which show a decay lifetime shape. Fig. 3 shows the same distributions for sectors off the K path. In the lower plots (times with respect to tpi), a strong photon peak with 2ns sigma is present, about 2ns after tpi for the rejection samples only. A decay lifetime shape for the same samples is present in the upper plots (time with respect to tk). Fig. 4 and fig. 5 show the same for the CCDs, which have a similar mean (-0.19) and resolution (0.6ns for the K peak and 2.5ns for the photon one) and a smaller shift (1.3ns) with respect to tpi. This is probably because the CCD time is the one at the 40% rising point of the pulse, returned by pulse.f. The photon time distributions for Kp2 peak events and kinks are compared in fig. 6, where it can be seen that there is more photon activity in the AD for kinks.
Time vs energy distributions for the same samples are shown in fig. 7 (fig. 8 for CCDs) and energy distributions for the 2 timing peaks in fig. 9 (fig. 10 for CCDs). The K energy peak in time with tk is prominent, whereas most of the energy in time with tpi is near zero, with long high-energy tails, as expected for showering photons.
In addition to the photon peak in fig. 3, some K activity remnants in time with tk are present, that are the same for all samples. These are due to the inefficiencies in calculating the K path mentioned

earlier. To investigate further, fig. 11 shows the time distributions of the TDC and CCD hit closest to tk in every sector, for sectors on or off the Kaon path, for Km21's and Kp2 peak. The black and red histograms have the same number of events, but the "off path" ones have many more overflows, due to sectors with no activity at all, that have been ommitted for plotting purposes. The fraction of "on path" sectors that do not have a hit in time with tk (defined as within 4ns of tk) give the false sector assignment percentage. The fraction of "off path" sectors with a hit in time with tk give the inefficiency of the method. The results are shown in table 1.

	Km21		Kp2 peak	
	TDC	CCD	TDC	CCD
False assignment	18%	43%	20%	45%
Inefficiency	2.5%	4.4%	3.1%	4.8%

Table 1: The false sector assignment rate and the inefficiency of the K path finding algorithm, calculated from TDC and CCD data for Km21's and Kp2 peak.

The 2ns shift of the photon timing peak from tpi has been extensively investigated (remember, the Kaon peak is almost in time with tk). Fig. 12 shows the dependence of the fitted peak position on tgz (and thus the distance the photons have to travel from the target until they reach the AD), for Kp2 peak events (B4EKZ has already been applied), which has a clear linear form. For both the TDCs and CCDs, the slope of the linear fit gives a reasonable speed of light value of about $3.3 \times 10^8 m/s$ and $2.7 \times 10^8 m/s$ respectively. The second point of the CCD plot was not included in the fit in order to get a reasonable value. From these results, the photon TOF accounts for about 1ns.

During the time slewing studies, it was noted that, although the energy spectra of the K's and the photons (see fig. 9 and 10) differ significantly, this effect does not account for the shift of the two timing peaks, as they are consistently different by 2ns at any restricted energy range.
The difference of tpi from the time of individual pi fibers does not show a systematic shift either, but it is dominated by the resolution (if the fibers closest to the vertex were consistently earlier than tpi, this would reveal a consistent difference between the real time that the photon was emitted and left a trace in the AD, and the average pion time, namely tpi). So, the remaining 1ns shift remains a mystery.

3 Applying the cut

Based on the time and energy distributions in the AD, different ways to apply a PV cut were investigated. The main idea is to add the energy deposited either in whole sectors (for ADCs) or individual hits (for CCDs) and veto events based on this sum. For the ADCs, the different schemes are using sectors (a) with TDC hits in time with tpi (-2ns to 8ns) (b) with TDC hits in time with tpi and no TDC hits at any other time (c) with TDC hits in time with tpi that are also out of the K path and (d) with TDC hits in time with tpi, no TDC hits at any other time, and are also out of the K path. For the CCDs, either CCD hits (a) in time with tpi or (b) in time with tpi and in sectors out of the K path were used. The results, in the form of acceptance*rejection vs energy threshold, are shown in fig. 13 for the Kp2 peak and in fig. 14 for the kinks. For both the rejection samples, cutting on the sum of CCD "energy" at 5., irrespective of the sector the hit belongs to, seems to be the favorable case. The rejection, acceptance and rejection*acceptance for the lowest energy threshold for all cases are summarized in table 2.

	ADC (a),(b)	ADC (c),(d)	CCD (a)	CCD (b)
acc	0.96±0.001	0.98±0.001	0.94±0.002	0.97±0.001
Kp2 peak				
rej	1.64±0.03	1.54±0.03	1.79±0.04	1.59±0.03
acc*rej	1.58±0.03	1.51±0.02	1.68±0.04	1.54±0.03
Kinks				
rej	1.81±0.07	1.73±0.05	1.95±0.08	1.80±0.07
acc*rej	1.76±0.08	1.70±0.06	1.86±0.08	1.76±0.08

Table 2: Rejection, acceptance and rej*acc of different implementations of the AD photon veto for both rejection samples, for the lowest thereshold (5.).

These rej*acc graphs also shed light on the question of how much photon activity is hidden under the Kaon sectors and how efficiently we can veto on it (losing the least acceptance) by using CCD pulse fits. It is evident that even if we veto on *any* activity at tpi in K sectors, the acceptance loss is offseted by the rejection gain. More detail is available in fig. 15 and fig. 16, which show the multiplicity (number of sectors hit) of the K, based on its extrapolated track and its timing, as well as the photon at TRS for KP2 peak events. 2 sectors on average are hit by the K and 2 by the gamma (with non-zero energy deposit). The number of sectors on the K path that have also non-zero energy hits at TRS is also shown, by itself and as a function of the total number of sectors with non-zero hits at TRS. Finally, the energy deposited in all sectors at TRS vs the energy only in the ones transversed by the Kaon is plotted. It turns out, from the number of events in the diagonal of the 2 last plots, which are the ones that all the photon activity is hidden under the Kaon, that, from the events that have photon energy hidden under the K sectors, only about 10% do not have significant energy outside these sectors to veto on.

4 Radial dependence of the energy

The dependence of the energy measured by the AD on the distance of the incoming track from the center of the detector was investigated. This is expected to vary by up to a factor of 2-3, as is shown in fig. 17, where the average of the ADC energy distribution of incoming Kaons is ploted vs the distance of the trace of the incoming particle left in the B4 from the center, for Km2 events where the track is confined in one sector. The same trend is present for the CCDs (fig. **??**), although the shape variation of the pulse with the distance from the readout may be to blame for the weakest dependence and the saturation for large distances (remember, the CCD "energy" is the pulse height).

References

[1] E787 TN375, "Simulation of elastic scatters of pi+ in the target from Kp2 decays".

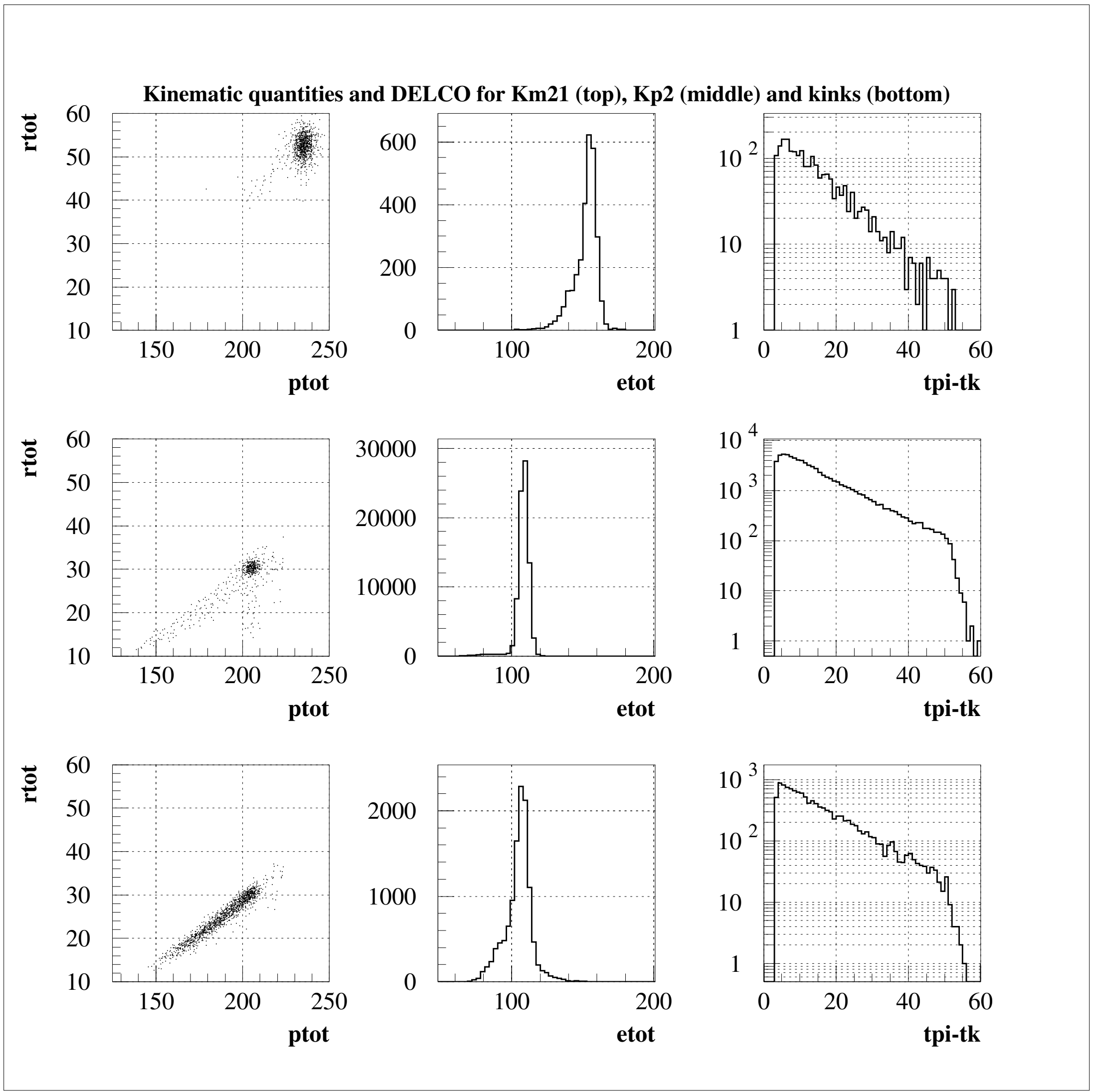

Figure 1: Kinematic distributions for the 3 samples used in this study: rtot vs ptot (left), etot (middle) and DELCO (right). The PV cut has not been applied for these plots, and for the 2 first columns the BOX cut has (obviously) not been applied either.

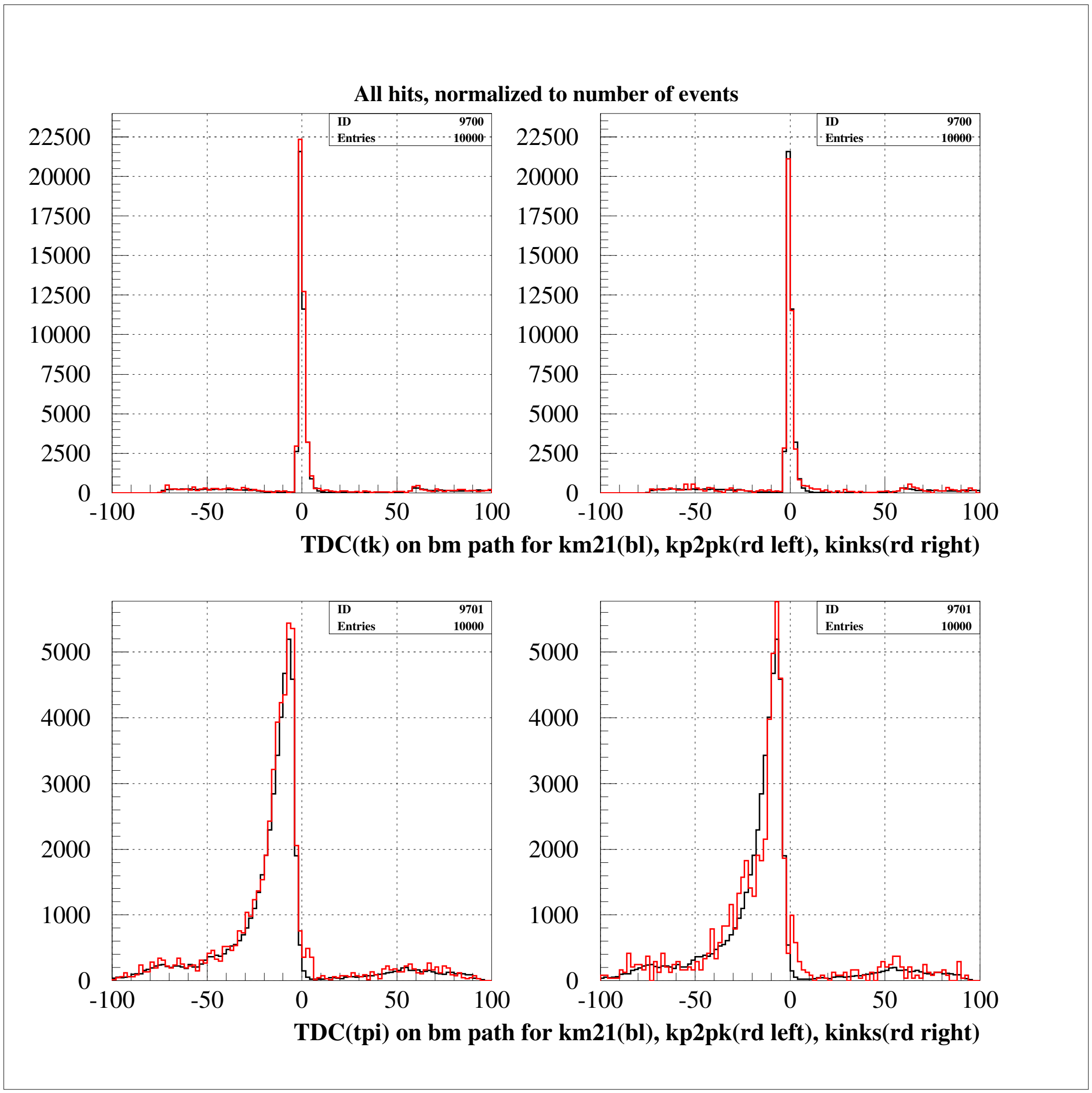

Figure 2: Time distributions of the TDC hits with respect to tk (top row) and tpi (bottom row) for sectors on the incoming Kaon path. Black histograms are for the acceptance sample (Km2 monitors) and red for the 2 rejection samples (Kp2peak on the left and kinks on the right).

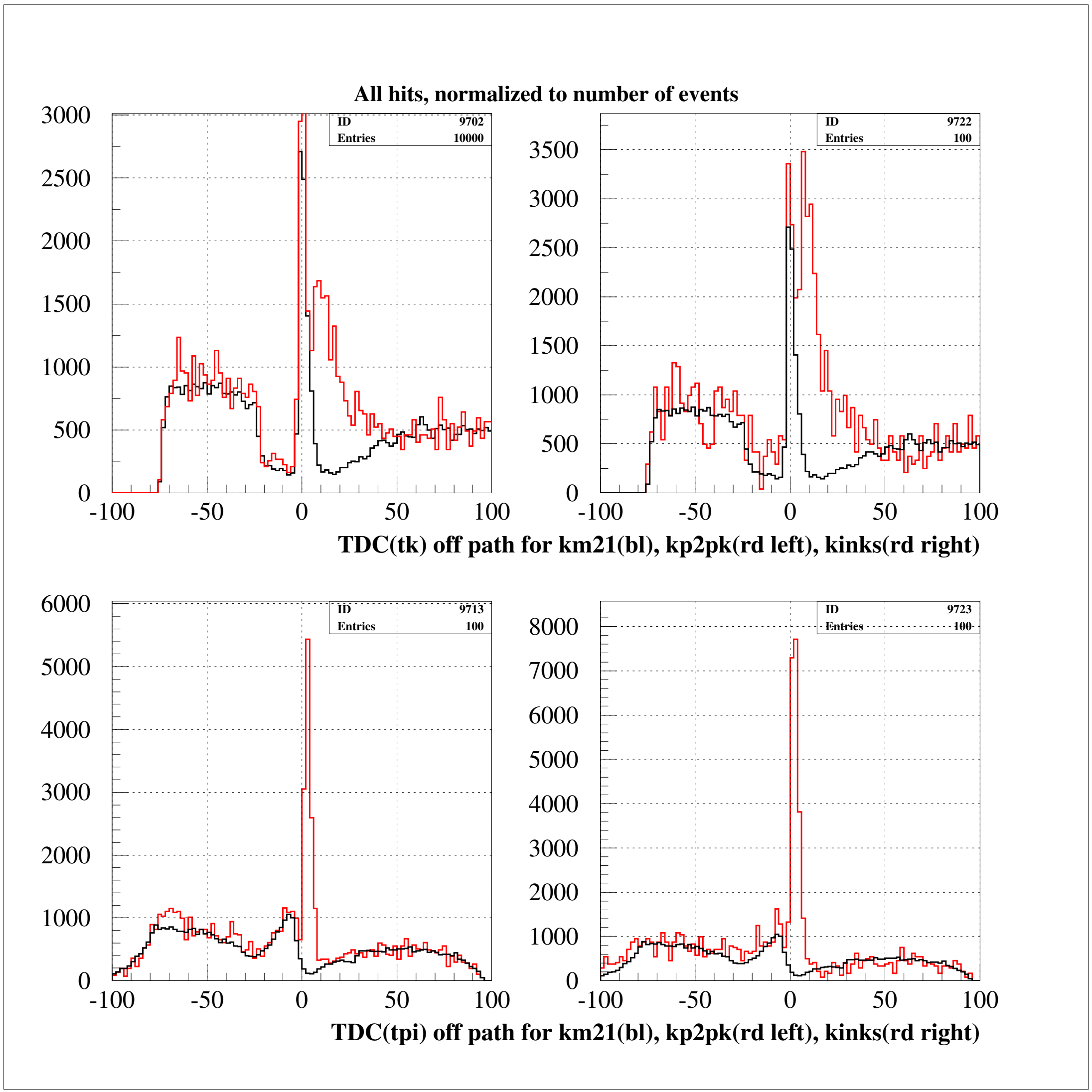

Figure 3: Time distributions of the TDC hits with respect to tk (top row) and tpi (bottom row) for sectors off the incoming Kaon path. Black histograms are for the acceptance sample (Km2 monitors) and red for the 2 rejection samples (Kp2peak on the left and kinks on the right).

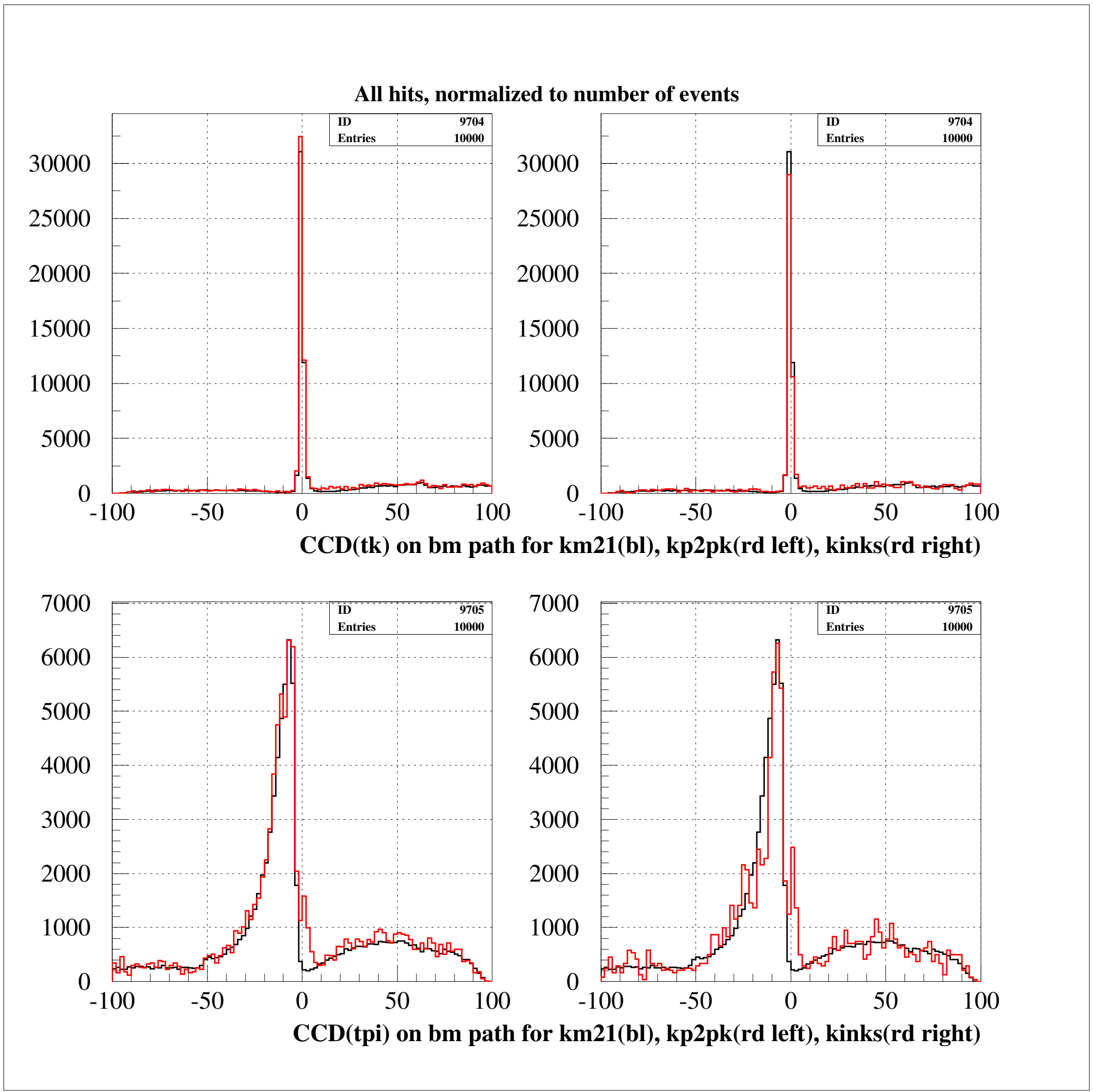

Figure 4: Time distributions of the CCD hits with respect to tk (top row) and tpi (bottom row) for sectors on the incoming Kaon path. Black histograms are for the acceptance sample (Km2 monitors) and red for the 2 rejection samples (Kp2peak on the left and kinks on the right).

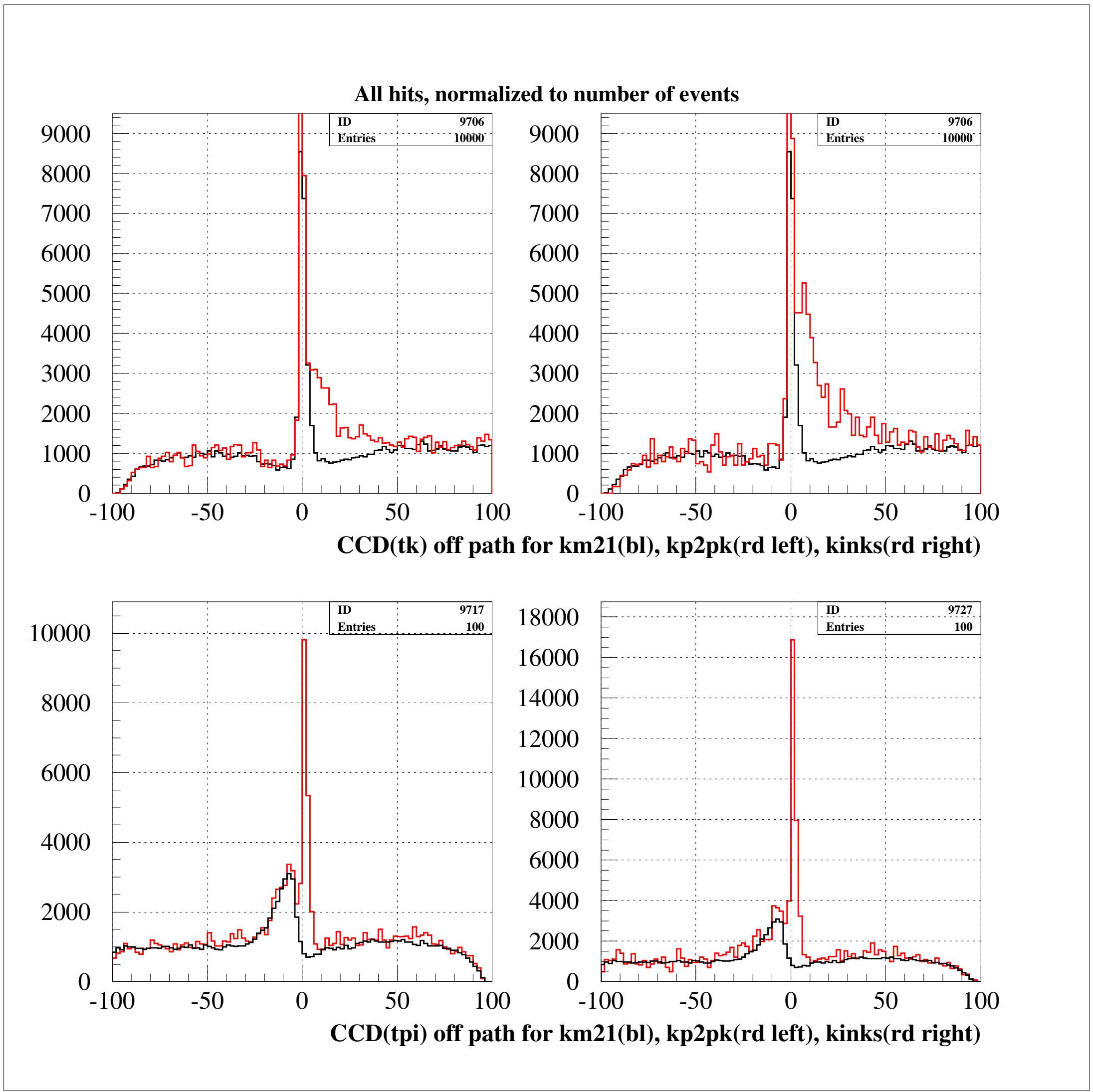

Figure 5: Time distributions of the CCD hits with respect to tk (top row) and tpi (bottom row) for sectors off the incoming Kaon path. Black histograms are for the acceptance sample (Km2 monitors) and red for the 2 rejection samples (Kp2peak on the left and kinks on the right).

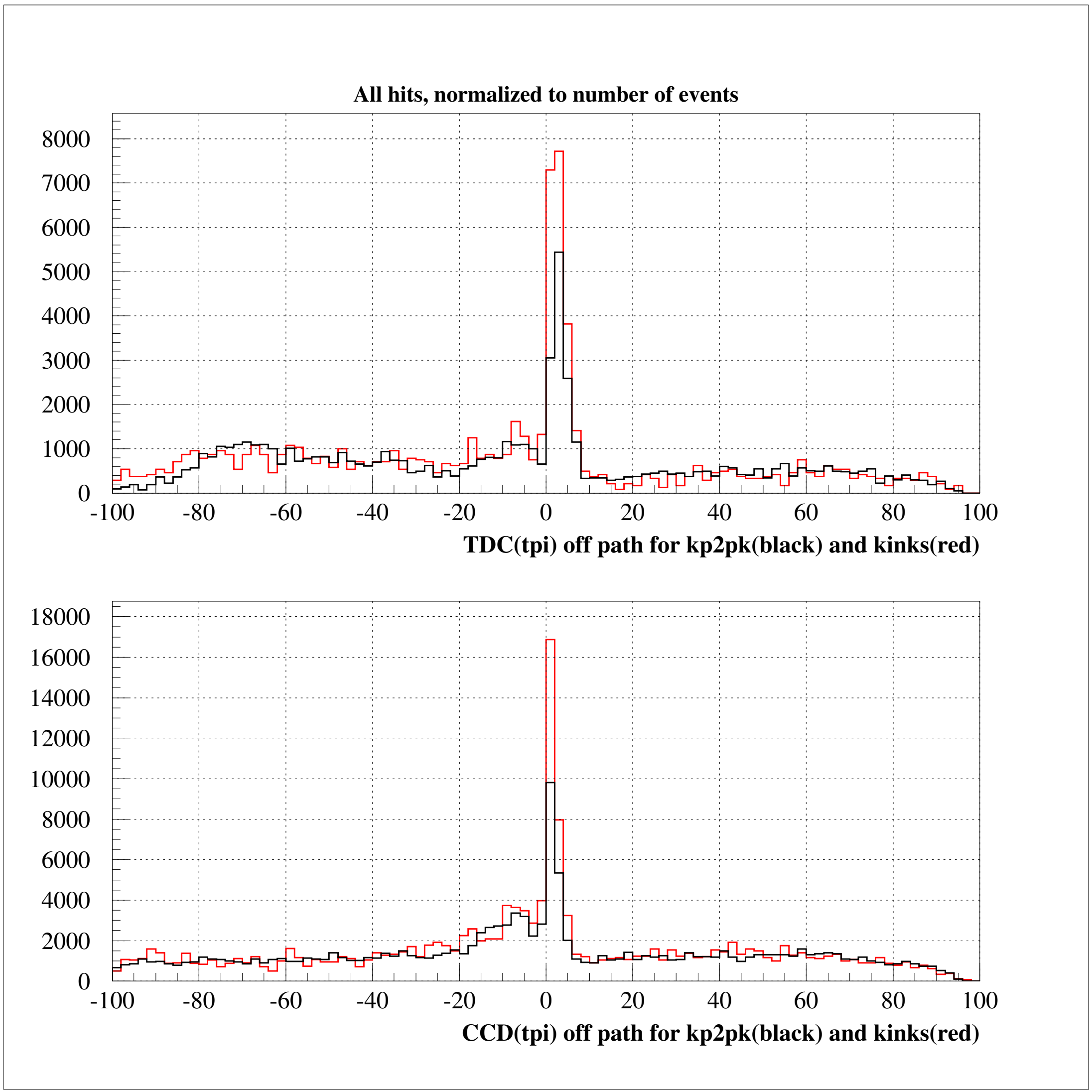

Figure 6: Time distributions with respect to tpi for sectors off the incoming Kaon path, from TDCs (top) and CCDs (bottom). Black histograms are for Kp2peak and red for kinks.

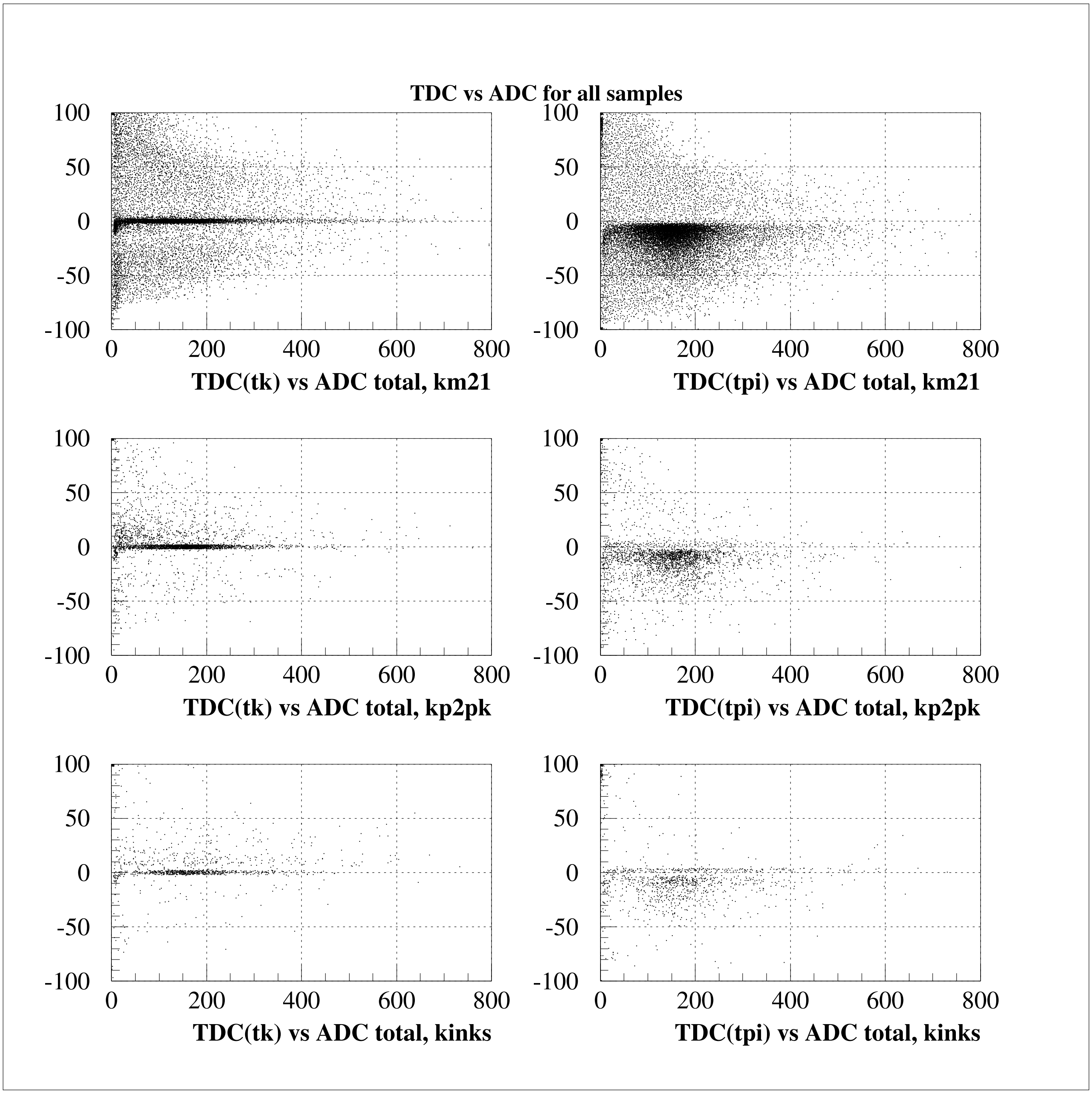

Figure 7: Time distributions with respect to tk (left) and tpi (right) of the TDC hit closest to tk or tpi, vs total ADC energy for Km21's (top), Kp2 peak (middle) and kinks (bottom).

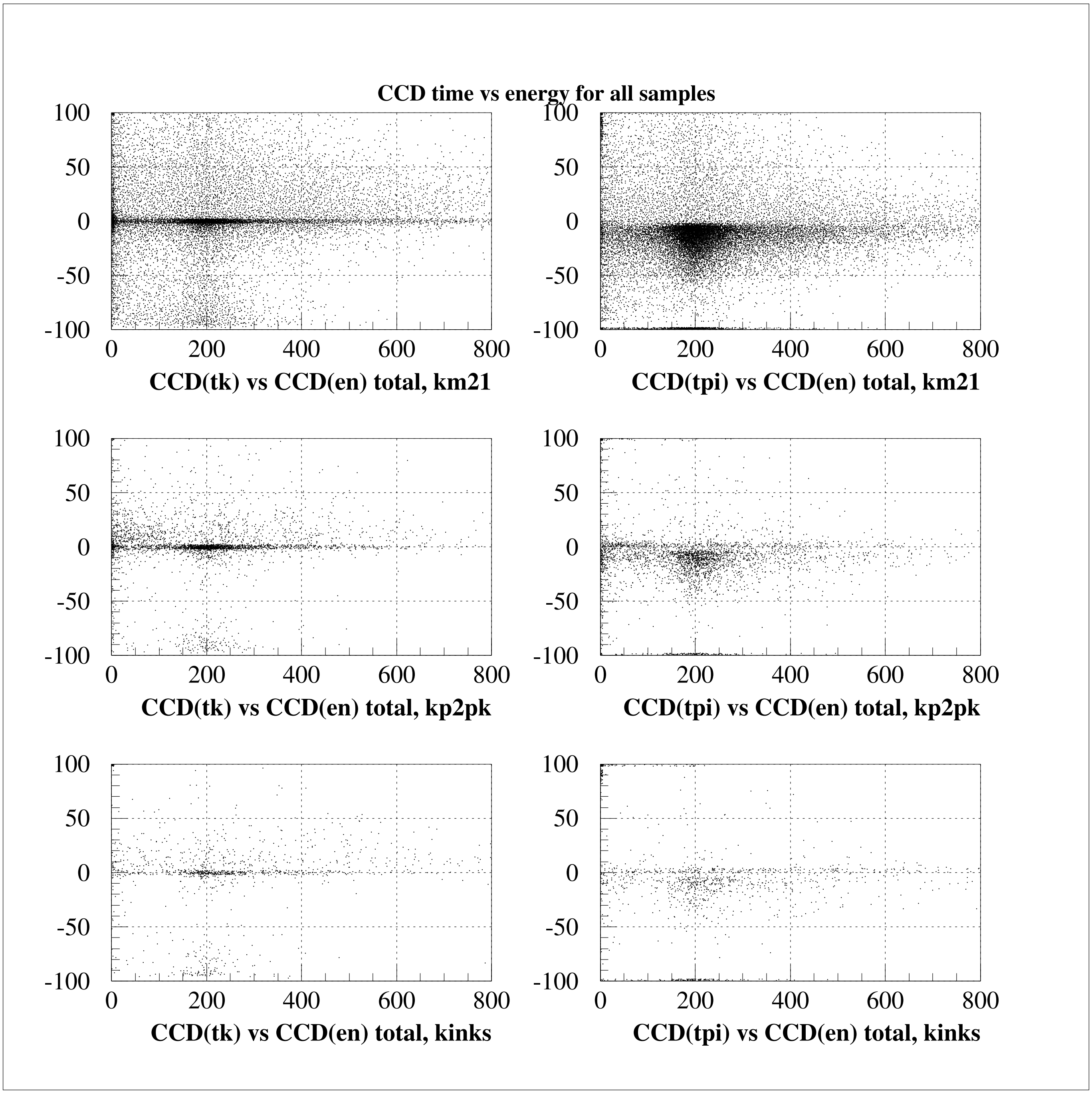

Figure 8: Time distributions with respect to tk (left) and tpi (right) of the CCD hit closest to tk or tpi, vs total CCD energy for Km21's (top), Kp2 peak (middle) and kinks (bottom).

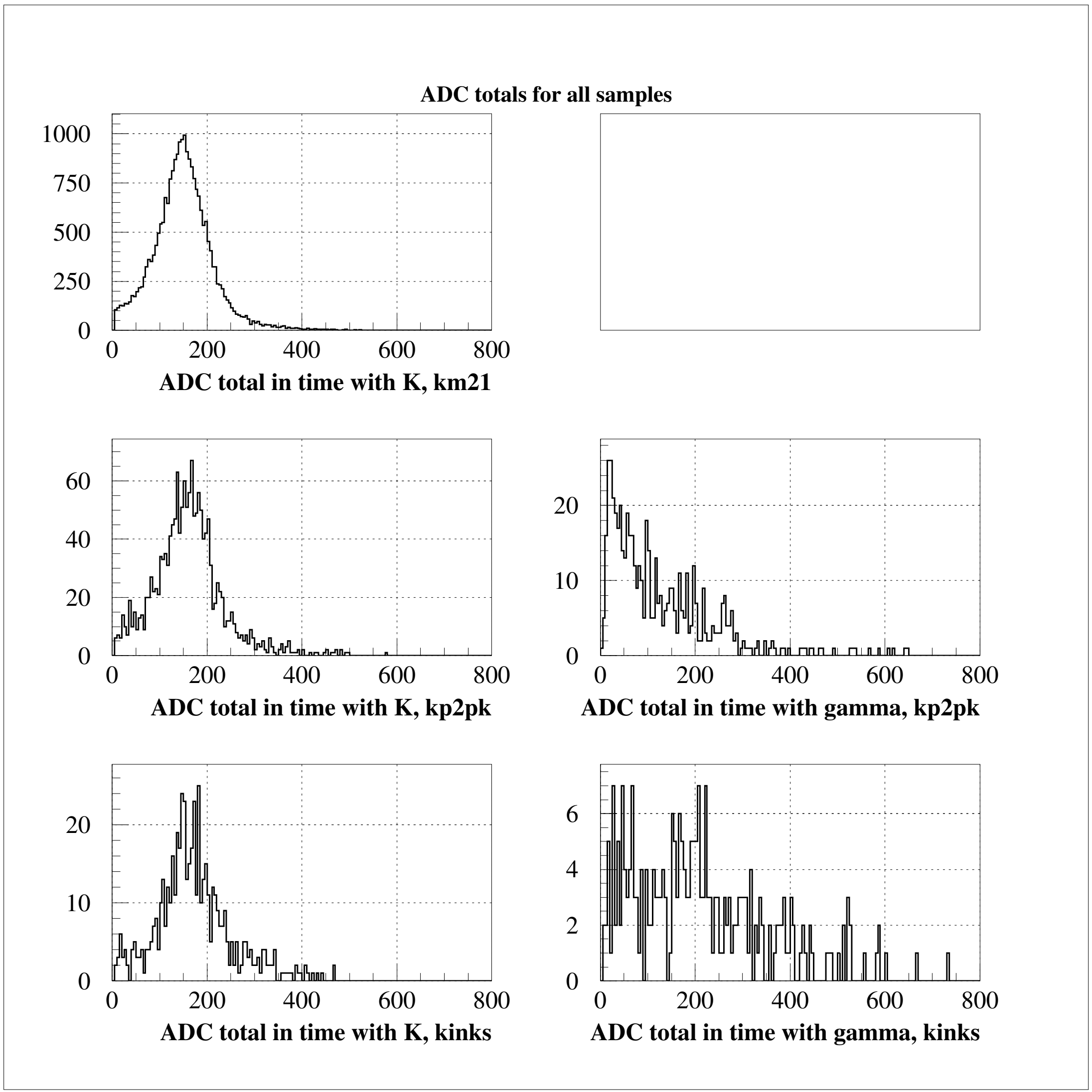

Figure 9: Total ADC energy in time with tk (left) and tpi (right) for Km21's (top), Kp2 peak (middle) and kinks (bottom).

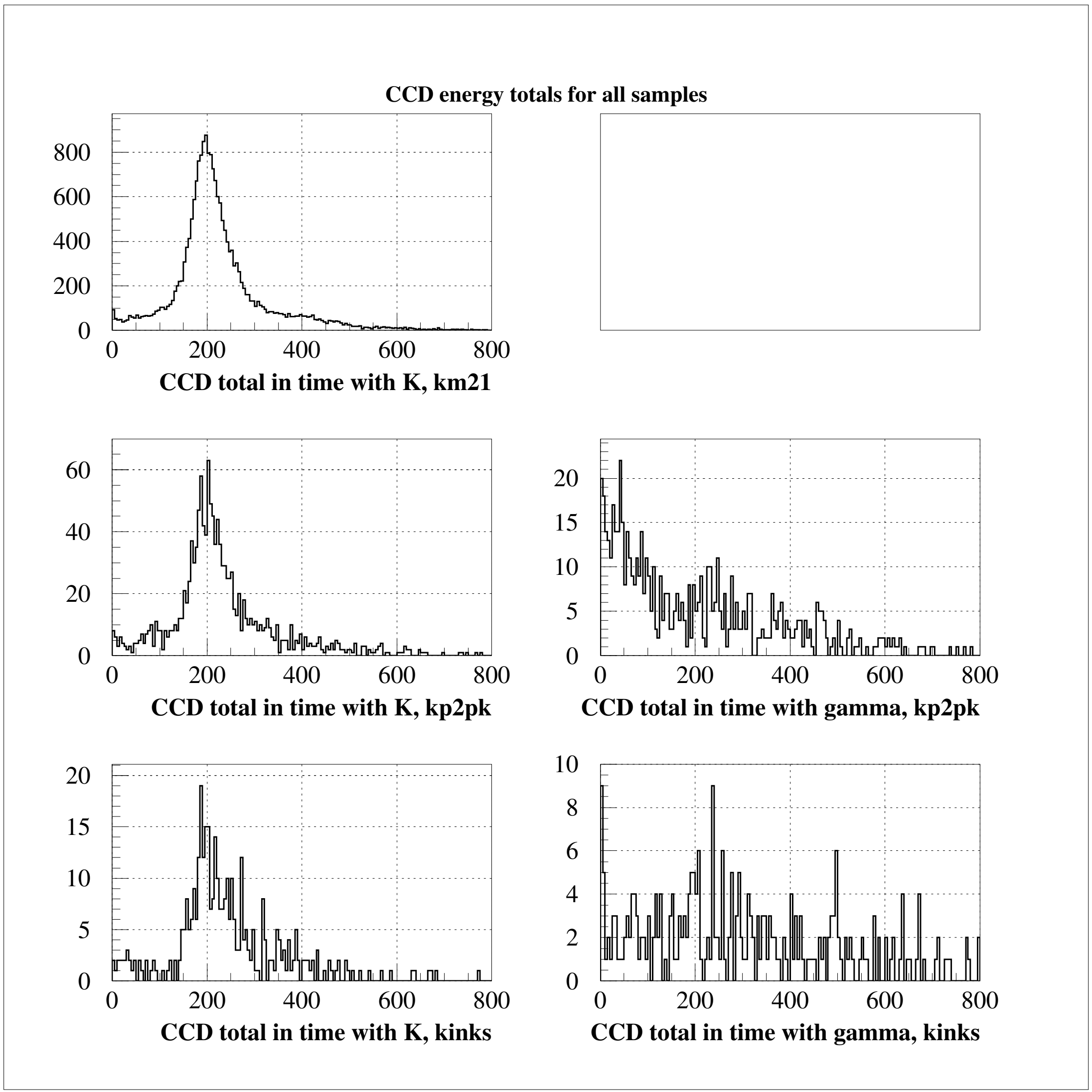

Figure 10: Total CCD energy in time with tk (left) and tpi (right) for Km21's (top), Kp2 peak (middle) and kinks (bottom).

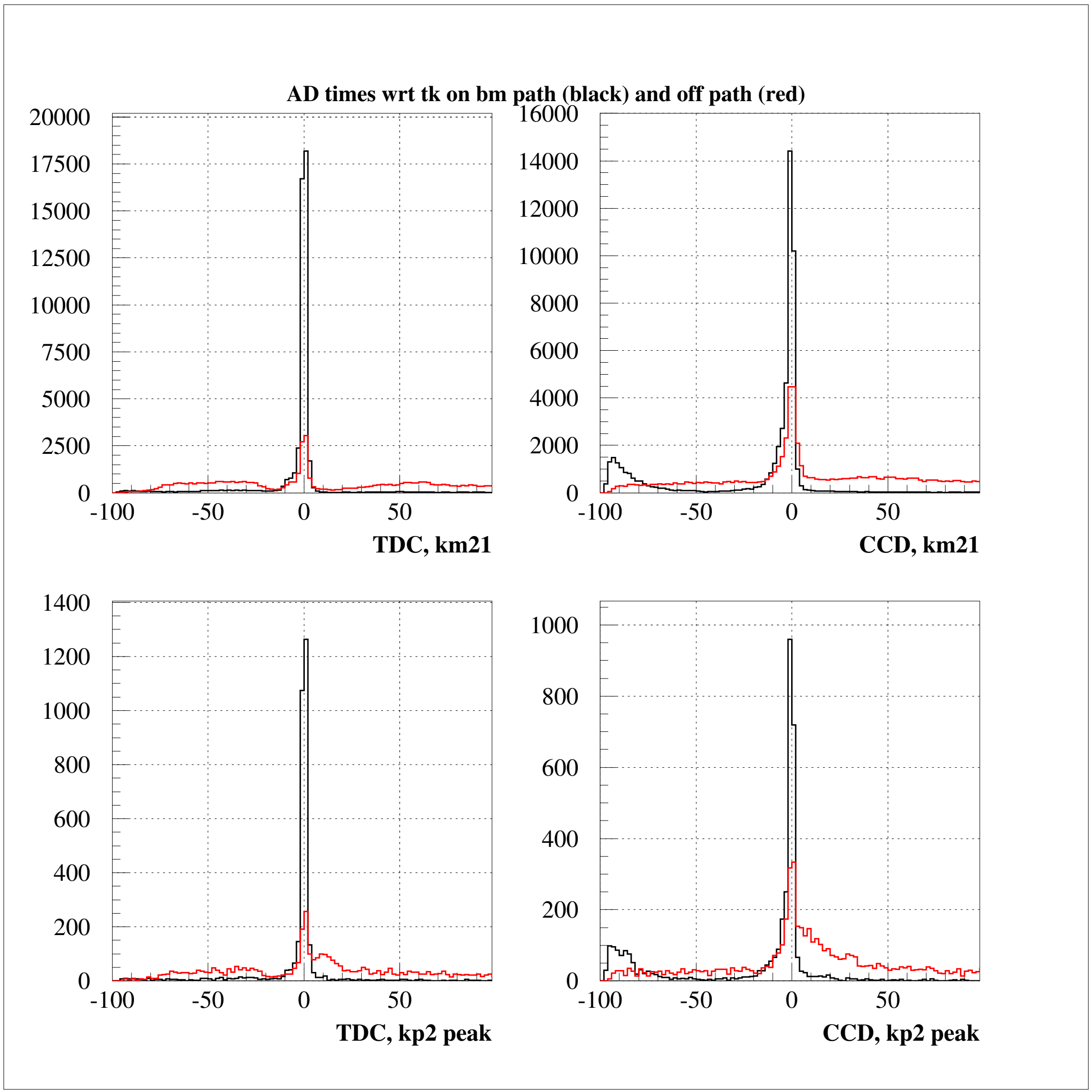

Figure 11: Time distributions with respect to tk of the TDC (left) and CCD (right) hit closest to tk in every sector, for sectors on (black) and off (red) the incoming Kaon path. The top row is for Km21's and the bottom row for Kp2 peak.

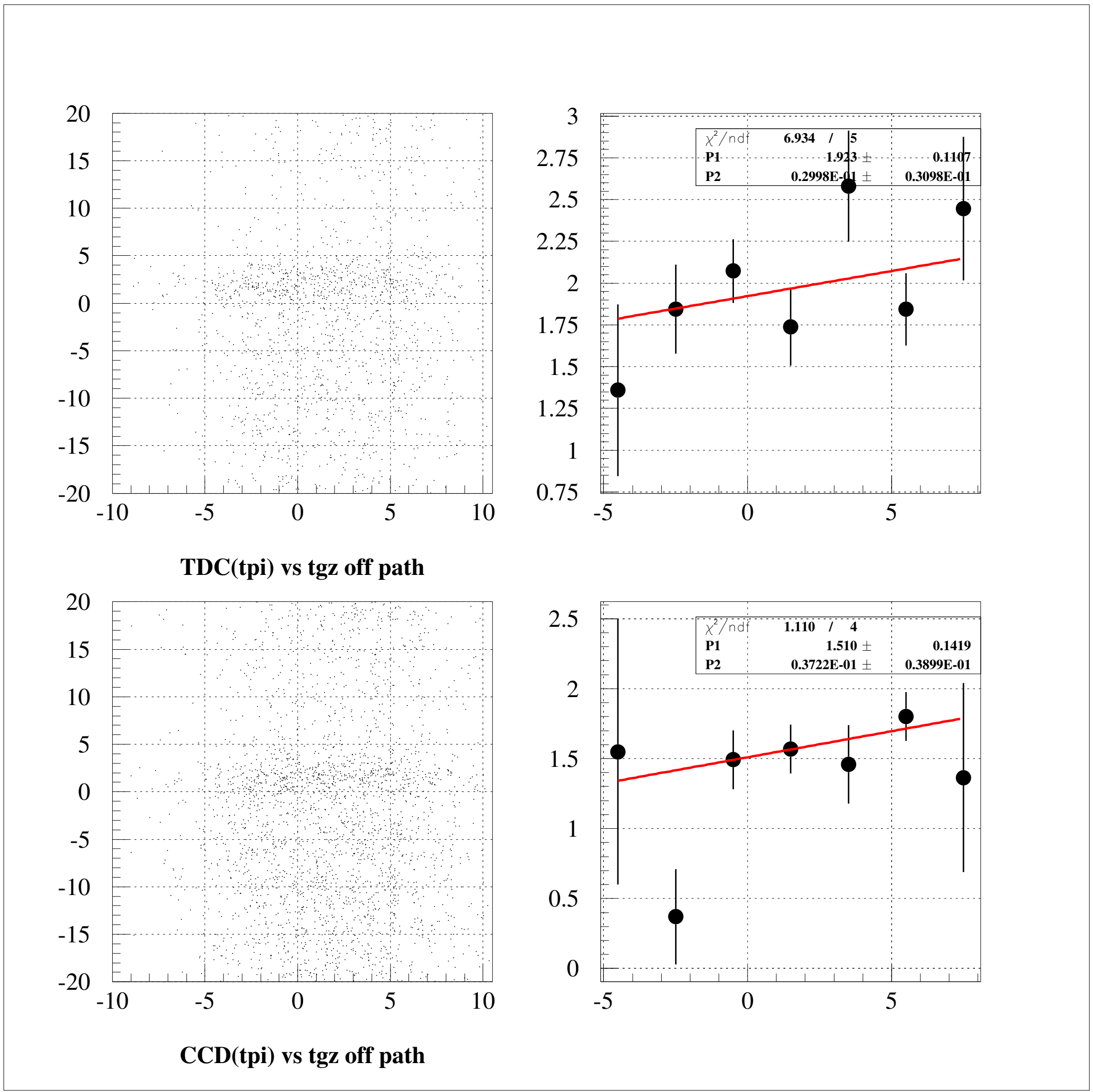

Figure 12: Dependence of the photon peak position in time with repsect to tpi, on tgz. Scatter plots (left) and the result of fitting the peak in the limits -2ns to 6ns vs tgz (right) are shown for the TDCs in the top and CCDs in the bottom row. The error bars are the errors in the fitted mean.

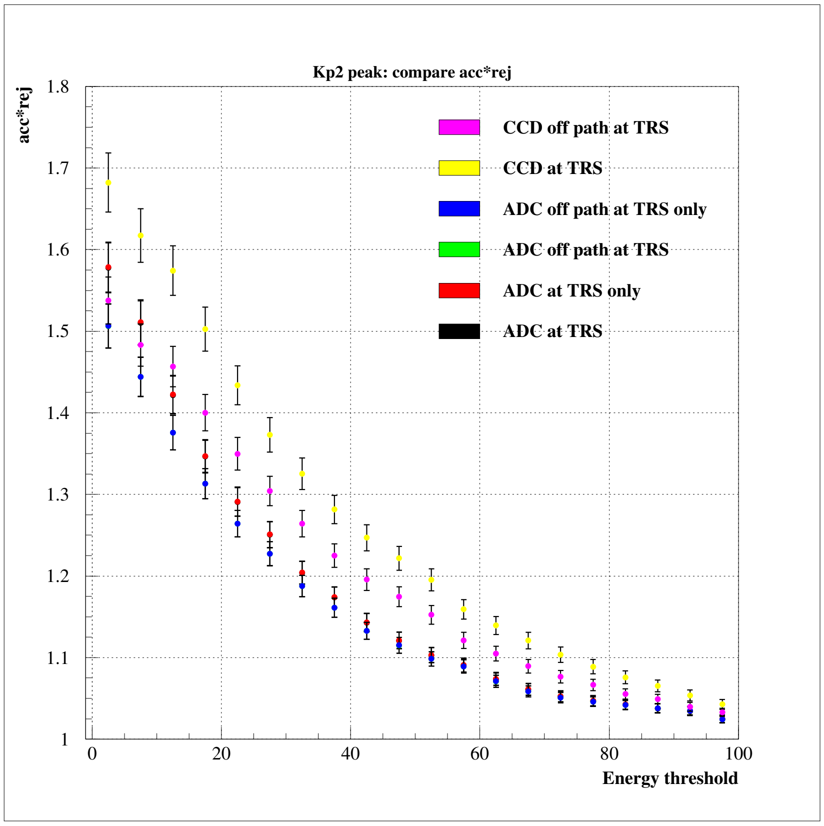

Figure 13: Acceptance*rejection vs total ADC or CCD energy threshold, for different sector selection, for Kp2 peak events. The different sets of points correspond to ADC cases a-d and CCD cases a-b explained in the text, from bottom to top. The points for ADC cases a and b, as well as c and d, completely overlap.

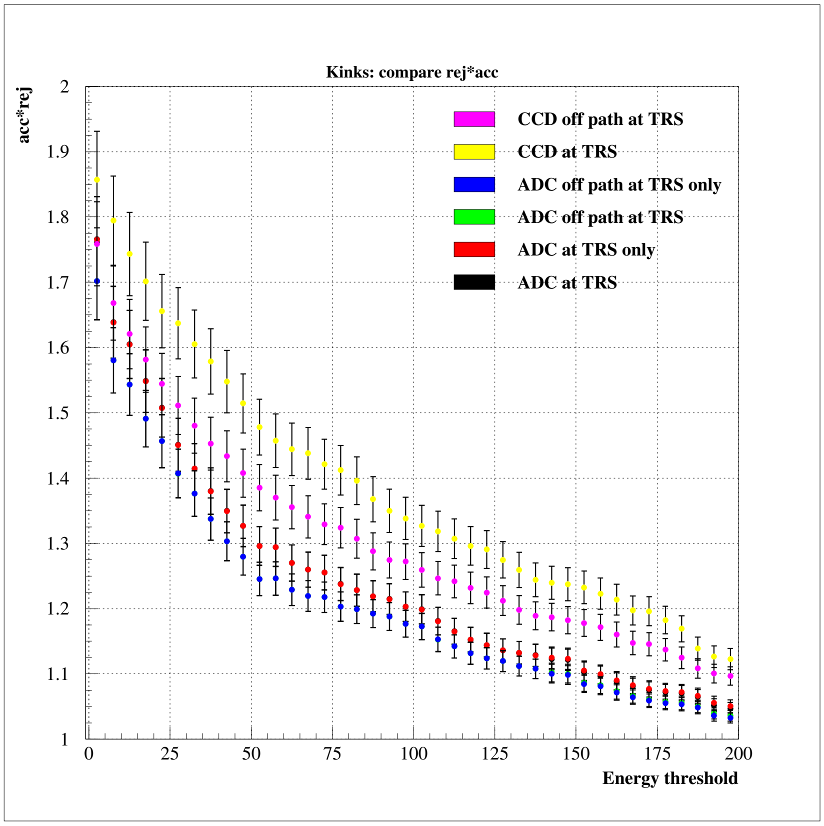

Figure 14: Acceptance*rejection vs total ADC or CCD energy threshold, for different sector selection, for kink events. The different sets of points correspond to ADC cases a-d and CCD cases a-b explained in the text, from bottom to top. The points for ADC cases a and b, as well as c and d, completely overlap.

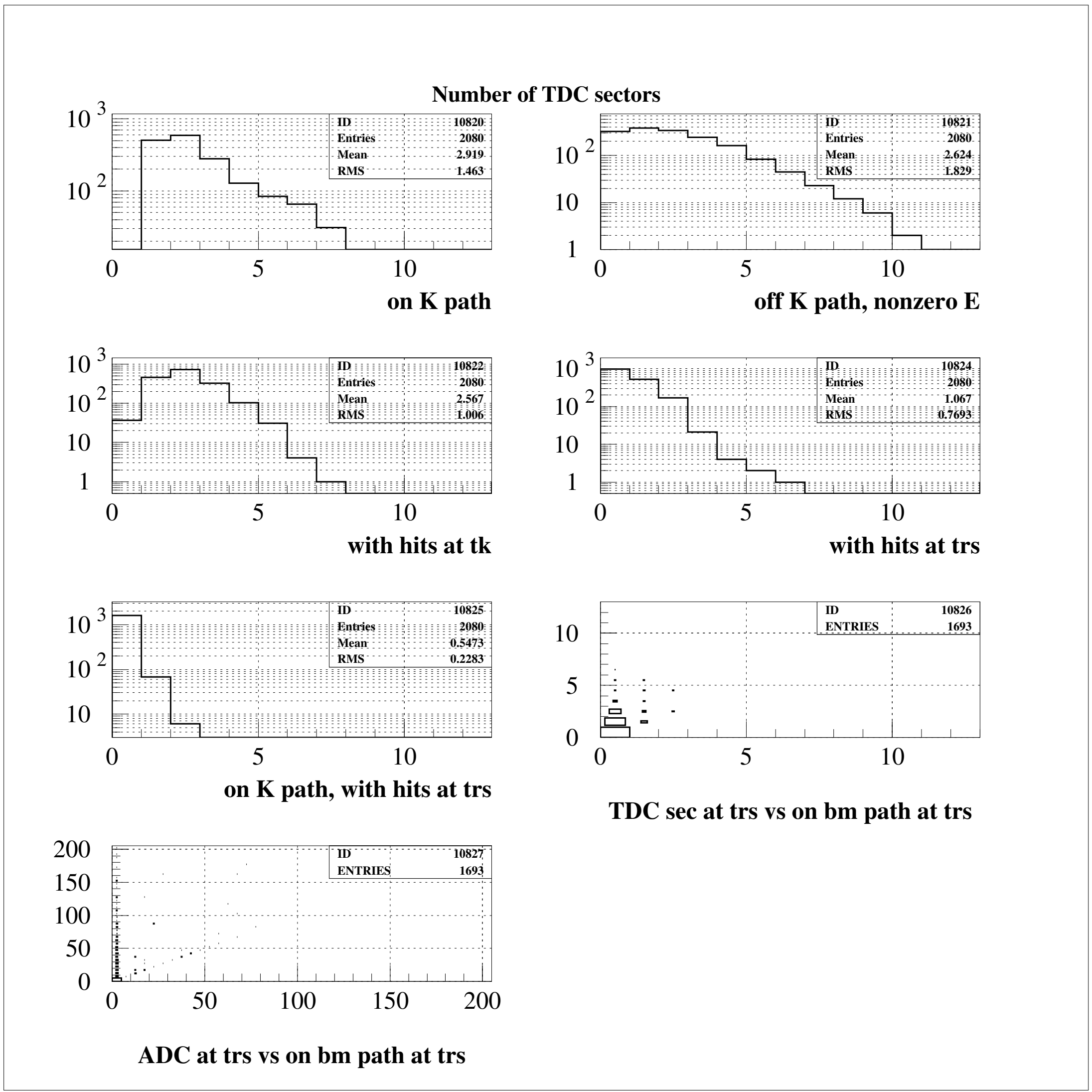

Figure 15: Number of sectors hit by incoming Kaons and outgoing photons for Kp2 peak: (a) on the extrapolated K path (b) off the extrapolated K path with non-zero ADC energy deposit (c) with TDC hits in time with tk (d) with TDC hits in time with TRS (e) with TDC hits in time with TRS on the extrapolated K path (f) number of sectors with TDC hits in time with TRS vs number of sectors with TDC hits in time with TRS on the extrapolated K path (g) total ADC energy deposited at sectors with hits at TRS vs total ADC energy deposited at sectors with hits at TRS on the K path.

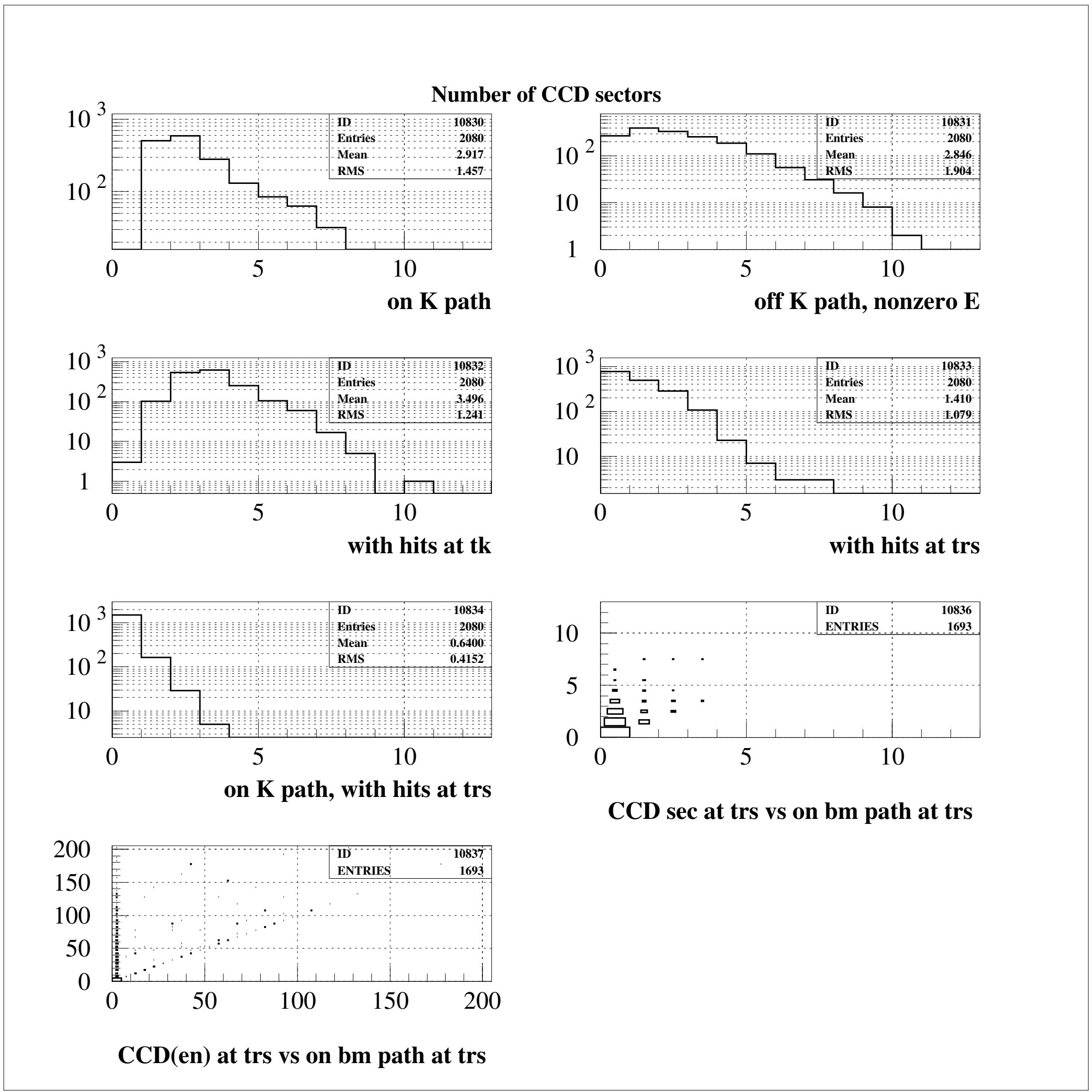

Figure 16: Number of sectors hit by incoming Kaons and outgoing photons for Kp2 peak: (a) on the extrapolated K path (b) off the extrapolated K path with non-zero CCD energy deposit (c) with CCD hits in time with tk (d) with CCD hits in time with TRS (e) with CCD hits in time with TRS on the extrapolated K path (f) number of sectors with CCD hits in time with TRS vs number of sectors with CCD hits in time with TRS on the extrapolated K path (g) total CCD energy deposited at sectors with hits at TRS vs total CCD energy deposited at sectors with hits at TRS on the K path.

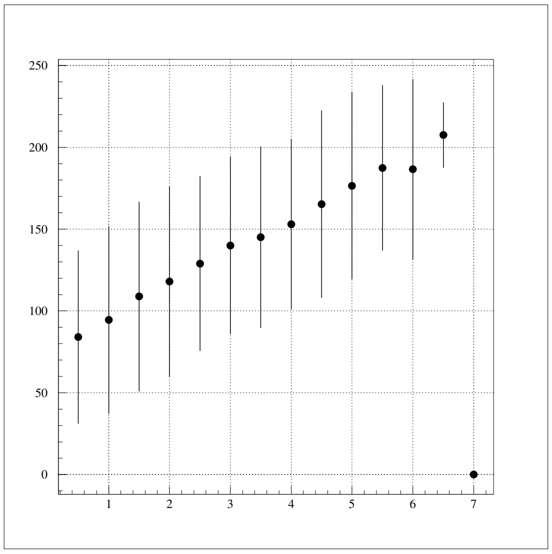

Figure 17: Average of the ADC energy distribution of incoming K's vs the distance of the trace of the incoming particle left in the B4 from the center. The error bars are the sigmas.